

## Article

# Blue Laser Irradiation Decreases the ATP Level in Mouse Skin and Increases the Production of Superoxide Anion and Hypochlorous Acid in Mouse Fibroblasts

Eiko Nakayama <sup>1,\*</sup> , Toshihiro Kushibiki <sup>2</sup> , Yoshine Mayumi <sup>2</sup>, Ryuichi Azuma <sup>1</sup>, Miya Ishihara <sup>2</sup>   
and Tomoharu Kiyosawa <sup>1</sup>

<sup>1</sup> Department of Plastic Surgery, National Defense Medical College, Saitama 3598513, Japan; azuma@ndmc.ac.jp (R.A.); xoo@ndmc.ac.jp (T.K.)

<sup>2</sup> Department of Medical Engineering, National Defense Medical College, Saitama 3598513, Japan; toshi@ndmc.ac.jp (T.K.); yoshine@ndmc.ac.jp (Y.M.); kobako@ndmc.ac.jp (M.I.)

\* Correspondence: dr31219@ndmc.ac.jp; Tel.: +81-4-2995-1596

**Simple Summary:** Photobiomodulation studies have reported that blue light irradiation induces the production of reactive oxygen species. We examined the effect of blue laser (405 nm) irradiation on ATP level in the skin and measured the types of reactive oxygen species and reactive nitrogen species. The decrease in the skin ATP level due to blue light irradiation may be caused by oxidative stress due to the generation of reactive oxygen species. These findings highlight the need to consider the effects on the skin when performing photobiomodulation treatment using blue light.



**Citation:** Nakayama, E.; Kushibiki, T.; Mayumi, Y.; Azuma, R.; Ishihara, M.; Kiyosawa, T. Blue Laser Irradiation Decreases the ATP Level in Mouse Skin and Increases the Production of Superoxide Anion and Hypochlorous Acid in Mouse Fibroblasts. *Biology* **2022**, *11*, 301. <https://doi.org/10.3390/biology11020301>

Academic Editors: Marcus Krüger, Sebastian M. Strauch and Peter Richter

Received: 7 January 2022

Accepted: 10 February 2022

Published: 12 February 2022

**Publisher's Note:** MDPI stays neutral with regard to jurisdictional claims in published maps and institutional affiliations.



**Copyright:** © 2022 by the authors. Licensee MDPI, Basel, Switzerland. This article is an open access article distributed under the terms and conditions of the Creative Commons Attribution (CC BY) license (<https://creativecommons.org/licenses/by/4.0/>).

**Abstract:** Photobiomodulation studies have reported that blue light irradiation induces the production of reactive oxygen species. We investigated the effect of blue laser (405 nm) irradiation on the ATP levels in mouse skin and determined the types of reactive oxygen species and reactive nitrogen species using cultured mouse fibroblasts. Blue laser irradiation caused a decrease in the ATP level in the mouse skin and triggered the generation of superoxide anion and hypochlorous acid, whereas nitric oxide and peroxynitrite were not detected. Moreover, blue laser irradiation resulted in reduced cell viability. It is believed that the decrease in the skin ATP level due to blue light irradiation results from the increased levels of oxidative stress due to the generation of reactive oxygen species. This method of systematically measuring the levels of reactive oxygen species and reactive nitrogen species may be useful for understanding the effects of irradiation conditions.

**Keywords:** photobiomodulation; laser; ATP; reactive oxygen species; reactive nitrogen species

## 1. Introduction

Under appropriate conditions, visible to near-infrared light irradiation exerts wound-healing, anti-inflammatory, anti-edema, and hair growth-promoting effects [1]. This phenomenon is called photobiomodulation (PBM). Light sources with wavelengths in the 400 nm range are used to treat psoriasis vulgaris, prurigo vulgaris, and atopy, as well as for tooth bleaching and restoration procedures involving composite resin [2–4]. In the treatment of acne vulgaris caused by *Cutibacterium acnes*, coproporphyrin III, a metabolite of *C. acnes*, acts as a photosensitizer. Reactive oxygen species (ROS) generated by irradiation with blue light can treat acne by sterilization [5]. The peak absorption of coproporphyrin III occurs at 415 nm and is effective in the presence of blue light [6]. Considering the therapeutic effects of blue light irradiation on acne, many practitioners perform irradiation for 10–20 min at an intensity of 30–90 mW/cm<sup>2</sup> [5]. Therefore, a certain irradiation level is required to obtain effective therapeutic outcomes. However, compared to ultraviolet light, visible light may be harmless to living organisms, and its effect on healthy tissues has not been extensively examined [7].

Some studies have reported that ROS and reactive nitrogen species (RNS) are produced in response to PBM [8]. ROS are produced in response to large doses of light, particularly blue light [9,10]. Previous studies have attempted to identify the ROS and RNS types that are produced in response to blue light [11,12]. Indeed, high ROS and RNS levels may be harmful to living organisms. Excessive ROS and RNS levels can permanently damage the DNA, resulting in aging and cancer [13]. Although the underlying mechanisms remain unknown, both ROS and RNS appear to play important roles in PBM [14]. ROS is a generic term for various molecules and free radicals (chemical species with one unpaired electron) that are derived from molecular oxygen. ROS comprise oxygen free radicals, such as the superoxide anion ( $O_2^{\cdot-}$ ) and hydroxyl radical ( $\cdot OH$ ), and non-radical oxidants, such as hydrogen peroxide ( $H_2O_2$ ), hypochlorous acid (HClO), and singlet oxygen ( $^1O_2$ ) [15].  $\cdot OH$  is highly reactive and acts very close to the generation site, whereas  $O_2^{\cdot-}$  and  $H_2O_2$  are less reactive [15]. RNS includes the relatively unreactive nitric oxide ( $NO$ ); its derivative, peroxynitrite ( $ONOO^-$ ), is a strong oxidant that can damage several biomolecules [15]. ROS and RNS are by-products of PBM and important second messengers [16]. ROS cause an increase in the intracellular redox potential and activates several intracellular signal transduction pathways, such as nucleic acid synthesis, protein synthesis, enzyme activation, and cell-cycle progression [14,17]. These pathways involve transcription factors, such as nuclear factor- $\kappa B$  (NF- $\kappa B$ ) and activator protein 1 (AP-1) [18]. NF- $\kappa B$ , a redox-regulated transcription factor, is a protein complex with multiple functions in the immune, inflammation, cell proliferation, and survival responses [17]. It induces the expression of inflammatory cytokines, such as interleukin (IL)-1, IL-2, IL-6, IL-8, IL-12, tumor necrosis factor- $\alpha$ , and interferon- $\gamma$ , and can regulate the cellular immune, inflammatory, stress, proliferation, and apoptotic responses [19]. In our previous study, mouse skin irradiation using a 415 nm light-emitting diode (LED) caused dermal fibroblast apoptosis (Supplementary Figure S1). To better understand these changes caused by ROS, a detailed study of the types and amounts of ROS generated by PBM is required.

Numerous fluorescent probes have been developed recently and are reported to distinguish the various ROS and RNS types produced in the cells. With the advent of these fluorescent probes, the process of detection has become easier, more detailed, and more intuitive. Therefore, measuring the ROS and RNS generated during the process could enable the evaluation of the reaction pathway induced by these species, which could aid in elucidating the underlying mechanisms of PBM.

To our knowledge, this is the first study to investigate the effect of blue laser irradiation on the tissues by evaluating the changes in the ATP level in the skin and to perform a detailed investigation of the generated ROS. Changes in the skin ATP levels in mice irradiated with a 405 nm blue laser (precisely, blue-violet) were measured using a firefly luciferase luminescence assay. Furthermore, we aimed to identify the types of ROS and RNS produced in response to blue laser irradiation in fibroblasts using multiple fluorescent probes. We used mouse fibroblasts because irradiation with blue light can damage the deep layers of the skin. Several ROS and RNS types were systematically measured using the same cells under the same experimental conditions.

## 2. Materials and Methods

### 2.1. Measurement of the ATP Levels in Mouse Skin

All animal experiments were conducted in compliance with the ARRIVE guidelines and in accordance with the relevant guidelines and regulations of National Defense Medical College. The study protocol was approved by the Ethics Committee for Animal Experiments of National Defense Medical College (approval number: 19010). The abdomen of each C57BL/6 mouse (Japan SLC Inc., Hamamatsu, Japan) was shaved a day prior to the experiment. The mice were anesthetized using 2% isoflurane (MSD Animal Health, Kenilworth, NJ, USA); the mice were placed in the supine position, and the abdomen was irradiated using a blue laser (100 or 30 mW/cm<sup>2</sup> for 20 min). The irradiation conditions were based on those used in clinical practice for PBM using blue light [20,21]. Skin tissues

(5 × 5 mm) were collected immediately after irradiation. The skin tissues on the opposite side of the same mice were considered the non-irradiated samples (control group). Tissue ATP assay Kit (TOYO B-Net, Tokyo, Japan) was used to evaluate the ATP levels in the mouse skin. The mouse skin tissues were homogenized using PBS containing 0.1% Triton X-100 (MP Biomedicals, Santa Ana, CA, USA) as a homogenate buffer. Subsequently, supernatants were collected after centrifuging at 15,000 rpm (174 × 100 g) for 5 min at 4 °C. The samples were processed according to the manufacturer's instructions, and luminescence levels were analyzed using a microplate reader (SpectraMax iD5; Molecular Devices, San Jose, CA, USA) to measure the ATP levels. To correct for variations in tissue volume, the protein content of each sample was measured using a TaKaRa BCA protein assay kit (item no. T9300A; TaKaRa Bio, Shiga, Japan), and the ATP levels were normalized to the protein content. The ATP levels are expressed as nmol/mg protein.

## 2.2. Cell Culture

L929 (American Type Culture Collection, Manassas, VA, USA) mouse fibroblasts of the subcutaneous connective tissue origin were used in this study. The cells were cultured in Dulbecco's modified Eagle medium (DMEM; Thermo Fisher Scientific, Waltham, MA, USA) containing 10% fetal bovine serum (FBS; Thermo Fisher Scientific), 100 units/mL penicillin, 0.25 µg/mL amphotericin B, and 0.1 mg/mL streptomycin (Antibiotic-Antimycotic; Thermo Fisher Scientific) at 37 °C in a 5% CO<sub>2</sub> atmosphere. L929 cells were seeded on a 96-well clear bottom culture plate (item no. 3860-096; AGC Techno Glass, Shizuoka, Japan) at a density of 4 × 10<sup>4</sup> cells/well, 1 day before light irradiation. For the 3-(4,5-dimethylthiazol-2-yl)-2,5-diphenyltetrazolium bromide (MTT) assay, similar seeding was performed at a density of 5 × 10<sup>3</sup> cells/well, 1 day preceding light irradiation. At the same time, the medium was changed to one lacking phenol red.

## 2.3. Fluorescent Probes for Detecting ROS and RNS

The intracellular ROS and RNS levels were measured by fluorescence analysis using five fluorescent probes. The details of these probes are presented in Table 1.

**Table 1.** Fluorescent probes used in the study and the ROS and RNS detected by each fluorescent probe.

Fluorescent Probe	Excitation (nm)/Emission (nm)	Detectable ROS and RNS <sup>a</sup>	Final Concentration	Incubation Time (min)	Positive Control Concentration	Supplier
OxiORANGE	543/577	•OH, HClO	1 µM	20	H <sub>2</sub> O <sub>2</sub> 500 µM	Goryo Chemical, Hokkaido, Japan
HySOx	555/575	HClO	5 µM	30	NaOCl 5 µM	Goryo Chemical
Dihydroethidium	518/606	O <sub>2</sub> <sup>•-</sup>	10 µM	30	Antimycin A 10 mM	Thermo Fisher Scientific
Nitrixyte Red	630/660	NO•	1 × <sup>b</sup>	30	NONOate 50 mM	AAT Bioquest, Sunnyvale, CA, USA
NiSPY-3	490/515	ONOO <sup>-</sup>	10 µM	30	Peroxynitrite 20 µM	Goryo Chemical

<sup>a</sup> •OH, hydroxyl radical; HClO, hypochlorous acid; O<sub>2</sub><sup>•-</sup>, superoxide anion; NO•, nitric oxide; ONOO<sup>-</sup>, peroxynitrite. <sup>b</sup> The purchased stock solution was diluted 500 times.

The cells were incubated in the dark at 37 °C with each of the fluorescent probes at the appropriate concentration and duration in DMEM-lacking FBS, antibiotics, and phenol red. After the incubation period, the cells were washed twice with Dulbecco's phosphate-buffered saline without calcium and magnesium (14190144; Thermo Fisher Scientific). Subsequently, the medium was changed to DMEM supplemented with FBS but lacking phenol red before the laser irradiations were performed.

#### 2.4. Laser Irradiation

A blue laser (RGBLase LLC, Fremont, CA, USA) with adjustable power (10–2000 mW) at a wavelength of 405 nm (continuous wave) was emitted directly from the fiber end at a distance of 5 cm from the surface of the mouse's abdomen. The irradiated area of the mouse's abdomen was a circle (diameter: 12 mm).

In the experiment using fibroblasts, the irradiated area in each well was 32.7 mm<sup>2</sup>. The cells were irradiated in the dark using a blue laser with a fiber attached to the bottom of the culture plate.

#### 2.5. Fluorescence Analyses

In our previous studies, we demonstrated that irradiation with visible light at an intensity of 30 or 100 mW/cm<sup>2</sup> significantly increased the ROS generation in different cell lines [22,23]. Moreover, a radiation intensity of 30–90 mW/cm<sup>2</sup> was found to be effective for the treatment of acne vulgaris [4]. In this research, dose selection was based on our previous research [22]. The fluorescent probe incorporated L929 cells that were irradiated with a 405 nm laser, from the bottom of each well, at 100 or 30 mW/cm<sup>2</sup> for 60 or 180 s. Fluorescent images were acquired using a fluorescence microscope (BZ-9000; Keyence, Osaka, Japan) pre- and post-laser irradiations. The cells were washed with PBS, treated with trypsin EDTA (0.25%) (Thermo Fisher Scientific) for dissociation, and subjected to flow cytometry (BD FACSCanto™ II; Becton, Dickinson and Company, Franklin Lakes, NJ, USA). The samples acquired for the fluorescence microscopy images were different from those that were used for flow cytometry. We used flow cytometry to measure the basal fluorescence of unstained cells and positive controls (Table 1). The mean fluorescence intensity (MFI) was determined for each cell group by analyzing  $>1 \times 10^4$  cells in each group. The MFI ratio was calculated by dividing the MFI of irradiated cells (designated as irradiated MFI) by that of non-irradiated cells on the same day (designated as control MFI) as follows:

$$\text{MFI ratio} = (\text{Irradiated MFI}) / (\text{Control MFI})$$

The measurements were performed on the same day due to daily MFI variation based on the cell state, including the degree of confluence and fluorescent probe uptake.

#### 2.6. MTT Assay

An MTT cell count kit (item no. 23506-80; Nacalai Tesque, Inc., Kyoto, Japan) was used to assess cell viability following blue laser irradiation. Cells were seeded at  $5 \times 10^3$ /well in 96-well plates and irradiated using a 405 nm laser from the bottom of each well at 100 or 30 mW/cm<sup>2</sup> for 60 or 180 s. The cells were subsequently left in the dark at 37 °C for 24 h. After incubation, 10 µL of MTT solution was added to each well, and the absorbances after 4 h were measured using the 450 nm filter of a microplate reader (SpectraMax iD5; Molecular Devices Corp., San Jose, CA, USA).

#### 2.7. Statistical Analysis

Statistical analyses were performed using JMP Pro 15 software (SAS Institute Japan; Tokyo, Japan). To measure the ATP levels of the mouse skin, the data were analyzed using the unpaired two-tailed t-test. The MFI ratios to detect ROS and RNS were determined using seven independent experiments; the results were analyzed using a sign test. The MTT assay was performed in five independent experiments. A *p*-value < 0.05 was considered statistically significant.

### 3. Results

#### 3.1. Blue Laser Irradiation Reduced the ATP Levels in the Mouse Skin

The ATP levels in the mouse skin were measured using firefly luciferase luminescence assay. The skin ATP levels were significantly decreased after 20 min of irradiation at 100 mW/cm<sup>2</sup> (Figure 1).

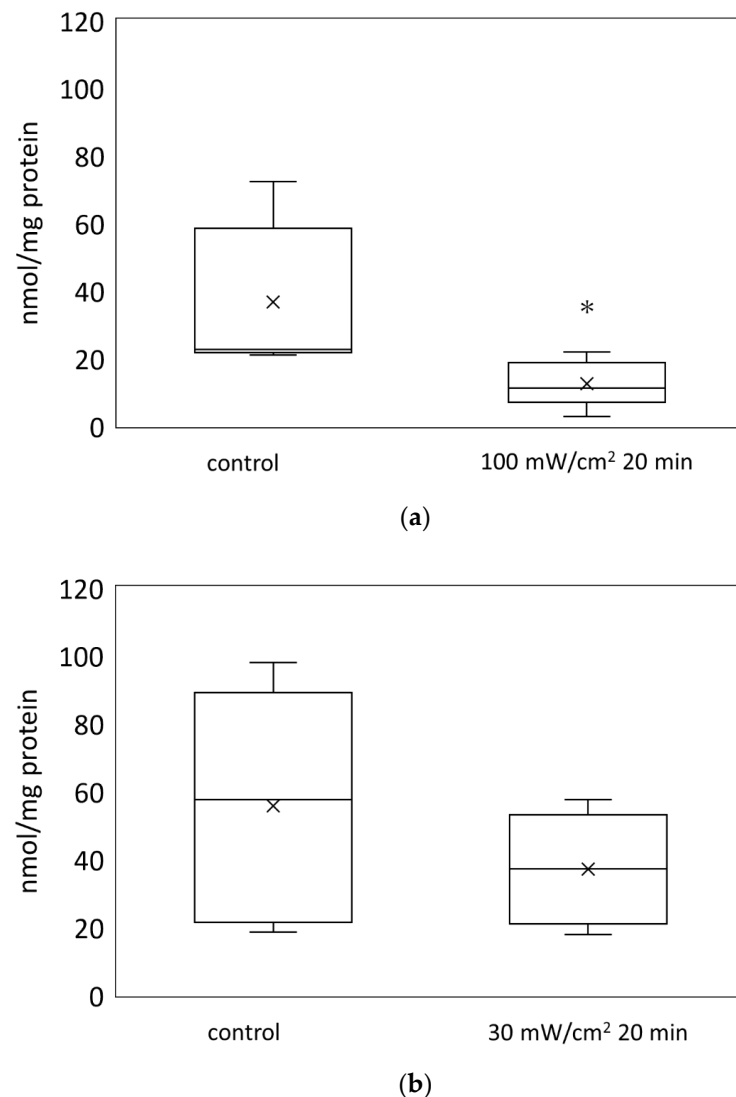
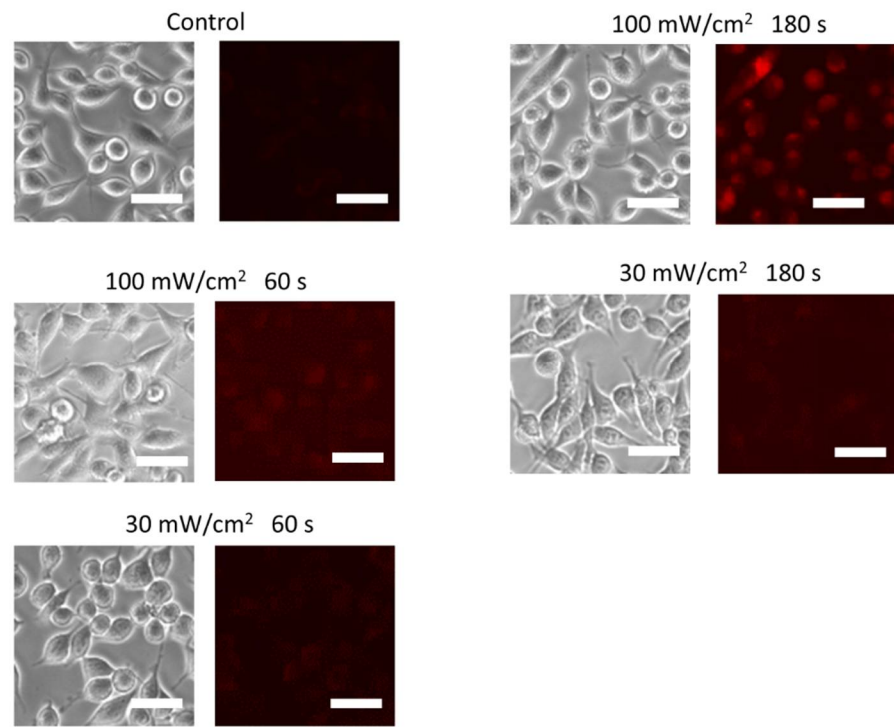


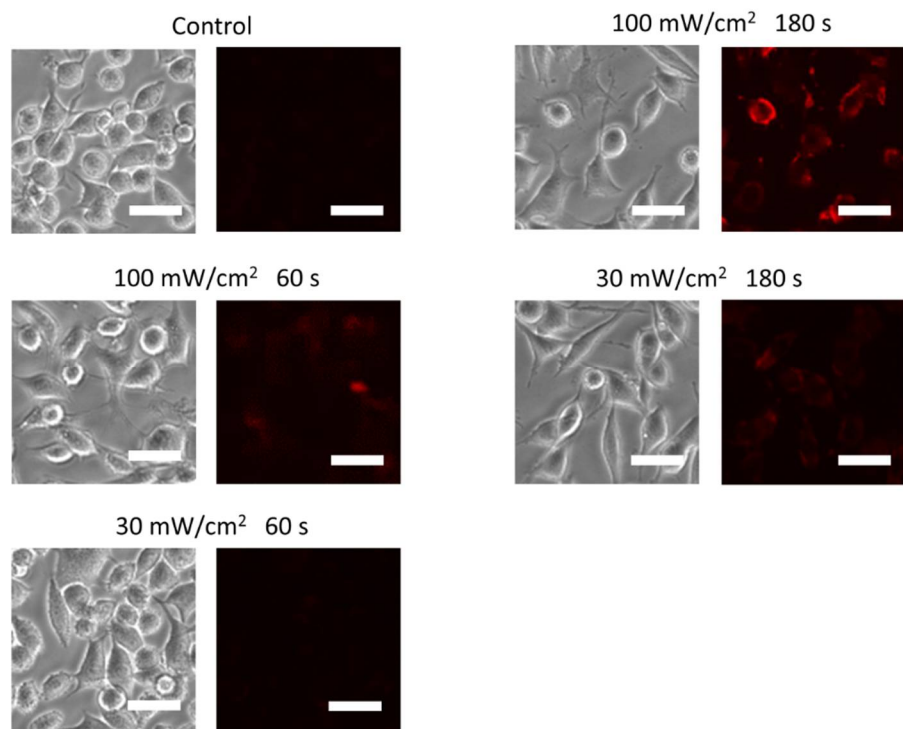
**Figure 1.** The ATP levels in the mouse skin after blue laser irradiation. The ATP levels in the mouse skin were measured using firefly luciferase luminescence assay. The irradiation conditions were (a) 100 mW/cm<sup>2</sup>, 20 min, 120 J and (b) 30 mW/cm<sup>2</sup>, 20 min, 36 J. \*  $p < 0.05$  against the control group.

### 3.2. Blue Laser Irradiation Induces the Generation of $O_2^{\cdot-}$ and HClO, but Not the Generation of $NO\bullet$ and $ONOO^-$

First, we assessed the ROS and RNS generation in L929 cells with incorporated fluorescent ROS and RNS detection probes after irradiation with a 405 nm blue laser, using fluorescence microscopy. Fluorescence intensities of OxiORANGE, which detects  $\bullet OH$  and HClO; HySOx, which detects HClO; and dihydroethidium, which relatively specifically detects  $O_2^{\cdot-}$ , significantly increased after comparison with those before irradiation (Figure 2). The highest fluorescence intensity was observed for dihydroethidium with 100 mW/cm<sup>2</sup> irradiation for 180 s. The fluorescence intensities of Nitrixyte Red, which detects  $NO\bullet$ , and NiSPY-3, which detects  $ONOO^-$ , remained unchanged following irradiation under the same conditions.

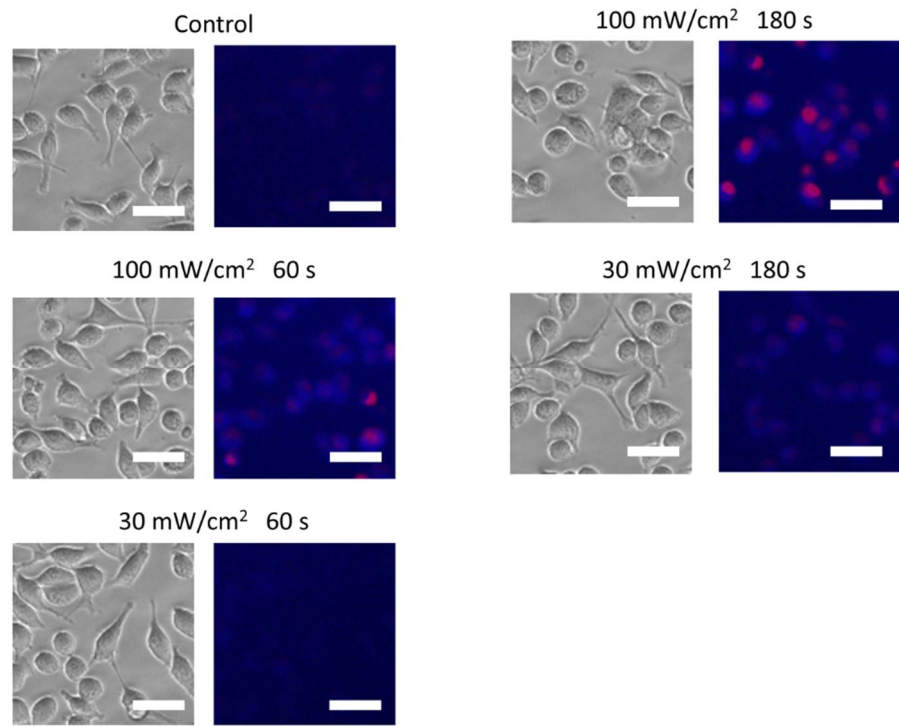


(a)

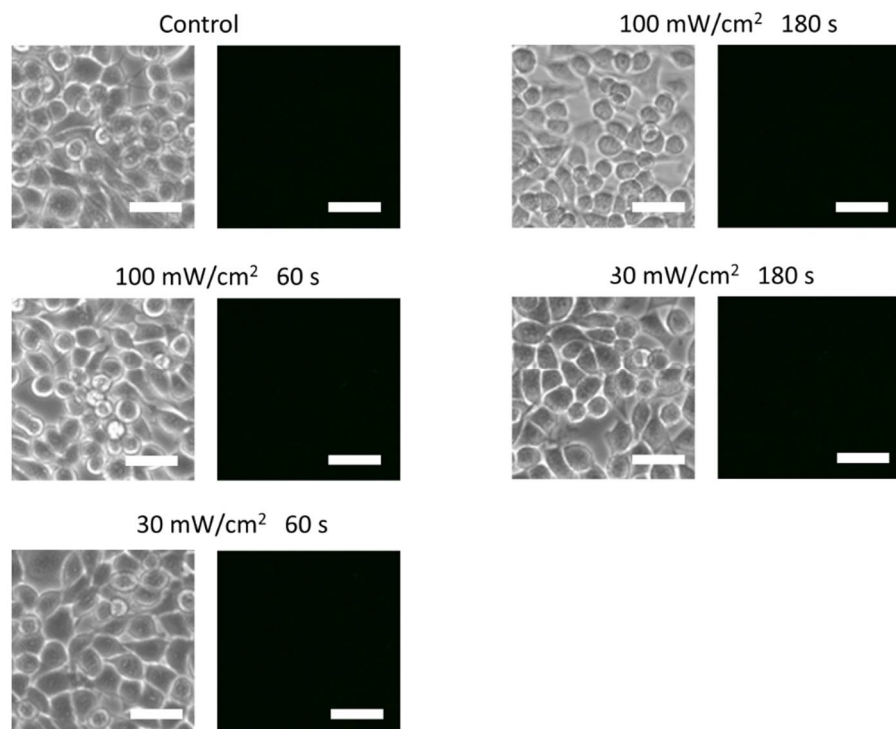


(b)

Figure 2. Cont.

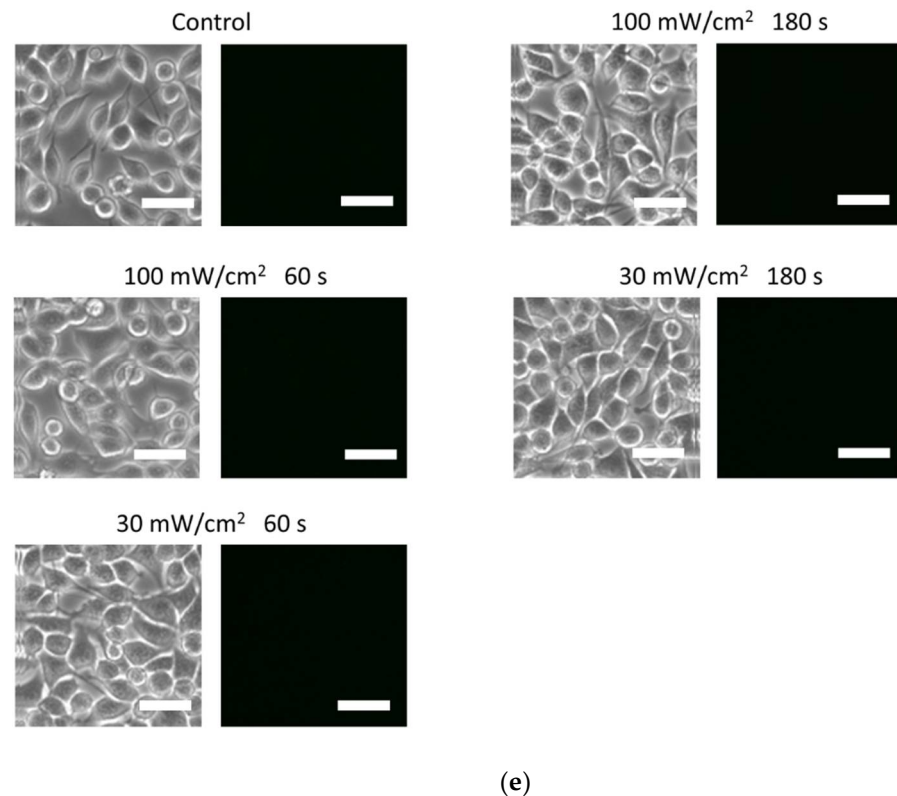


(c)



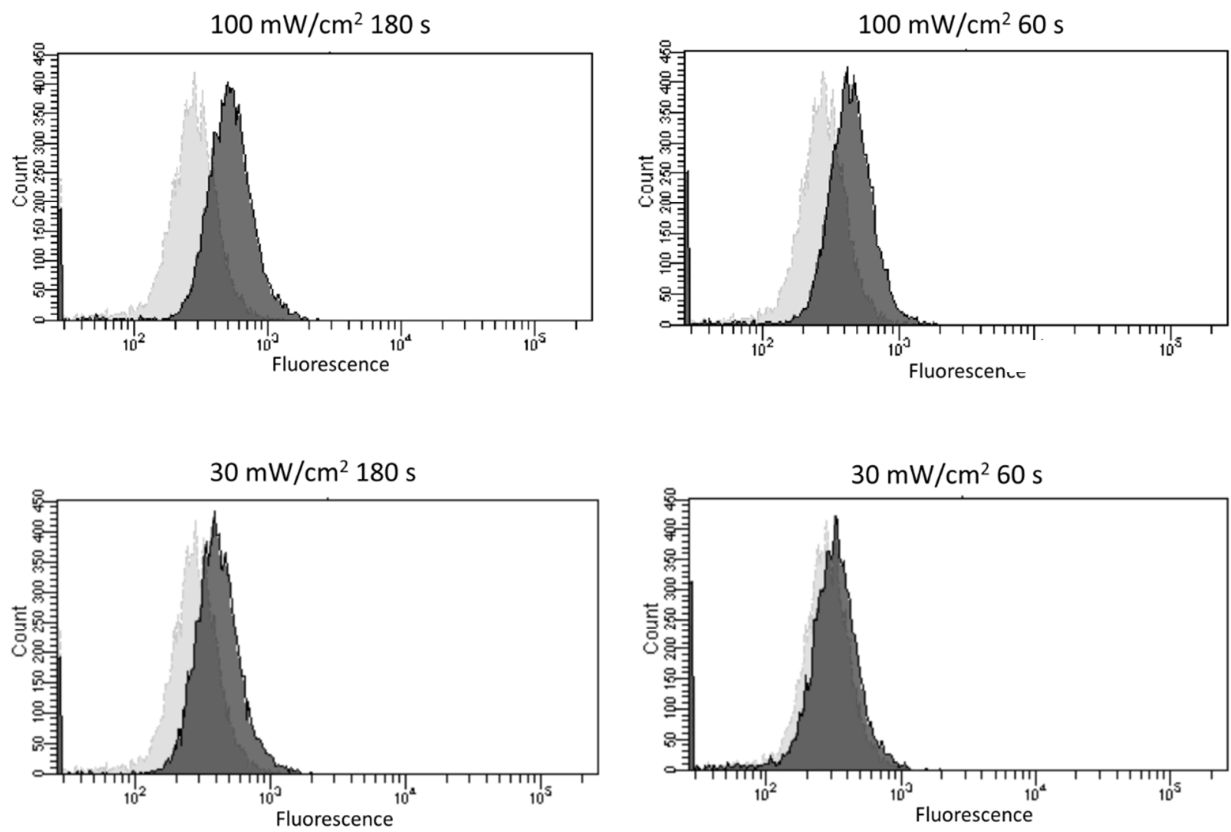
(d)

Figure 2. Cont.

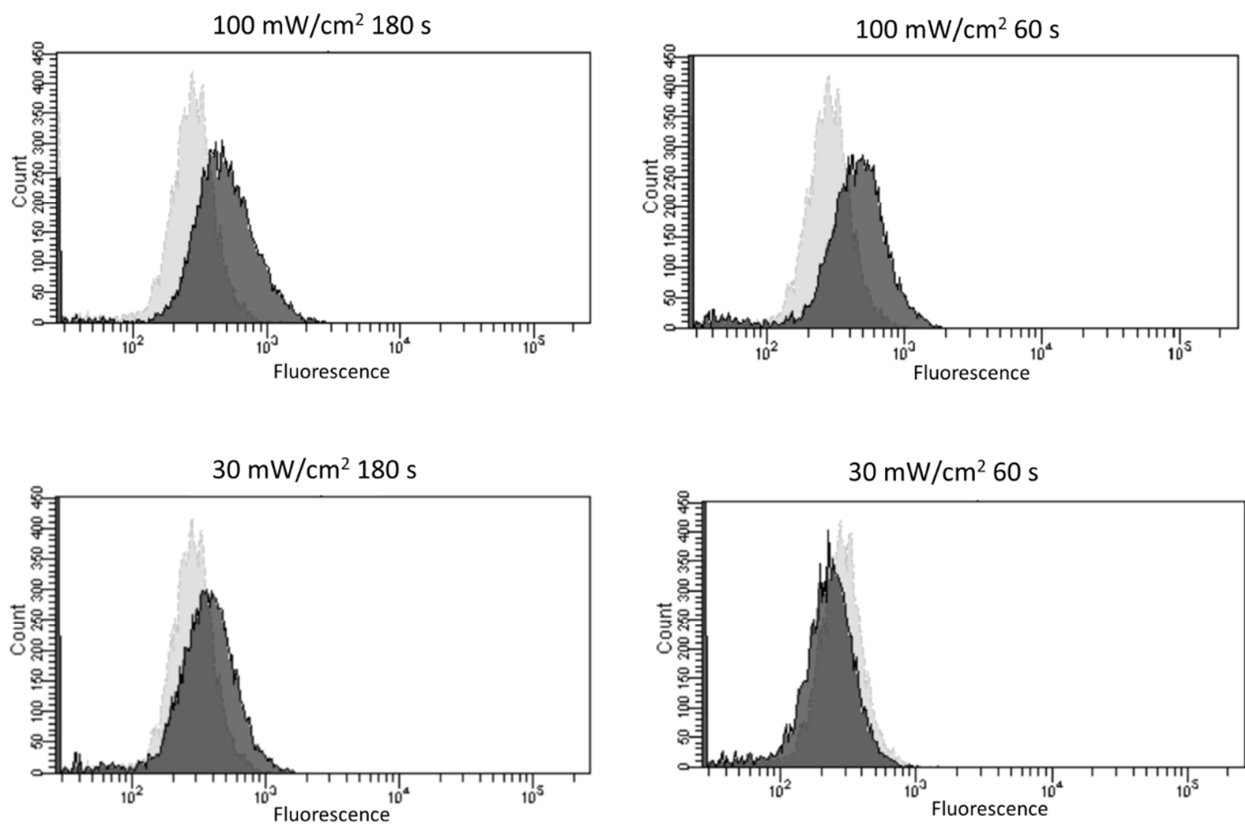


**Figure 2.** ROS and RNS generation after blue laser irradiation. Five fluorescent probes were incorporated into the L929 mouse fibroblasts. The cells were irradiated with a blue laser (405 nm), and the generation of ROS and RNS was evaluated using fluorescence microscopy. Phase-contrast microscopic images of the same sites are presented beside the fluorescent microscopic images. The fluorescent probes used were (a) OxiORANGE (detects  $\bullet\text{OH}$  and  $\text{HClO}$ ), (b) HySOx (detects  $\text{HClO}$ ), (c) dihydroethidium (detects  $\text{O}_2^{\bullet-}$ ), (d) Nitrixyte Red (detects  $\text{NO}\bullet$ ), and (e) NiSPY-3 (detects  $\text{ONOO}^-$ ). The irradiation conditions were as follows: (1) control, no laser irradiation; (2)  $100\text{ mW/cm}^2$ , 180 s, 18 J; (3)  $100\text{ mW/cm}^2$ , 60 s, 6 J; (4)  $30\text{ mW/cm}^2$ , 180 s, 5.4 J; (5)  $30\text{ mW/cm}^2$ , 60 s, 1.8 J. Scale bar =  $30\ \mu\text{m}$ .  $\bullet\text{OH}$ , hydroxyl radical;  $\text{HClO}$ , hypochlorous acid;  $\text{O}_2^{\bullet-}$ , superoxide anion;  $\text{NO}\bullet$ , nitric oxide;  $\text{ONOO}^-$ , peroxynitrite.

Figure 3 shows a representative histogram of the change in the fluorescence intensity obtained by flow cytometry when the cells incorporating each fluorescent probe were irradiated with a blue laser under various conditions. The light and dark gray histograms correspond to the non-irradiated and irradiated groups, respectively. In OxiORANGE (detects  $\bullet\text{OH}$  and  $\text{HClO}$ ), HySOX (detects  $\text{HClO}$ ), and dihydroethidium (detects  $\text{O}_2^{\bullet-}$ ), the peak of fluorescence intensity shifted mainly in the  $100\text{ mW/cm}^2$  irradiated group. When using Nitrixyte Red (detects  $\text{NO}\bullet$ ) and NiSPY-3 (detects  $\text{ONOO}^-$ ), no obvious shifts in the fluorescence brightness were observed.

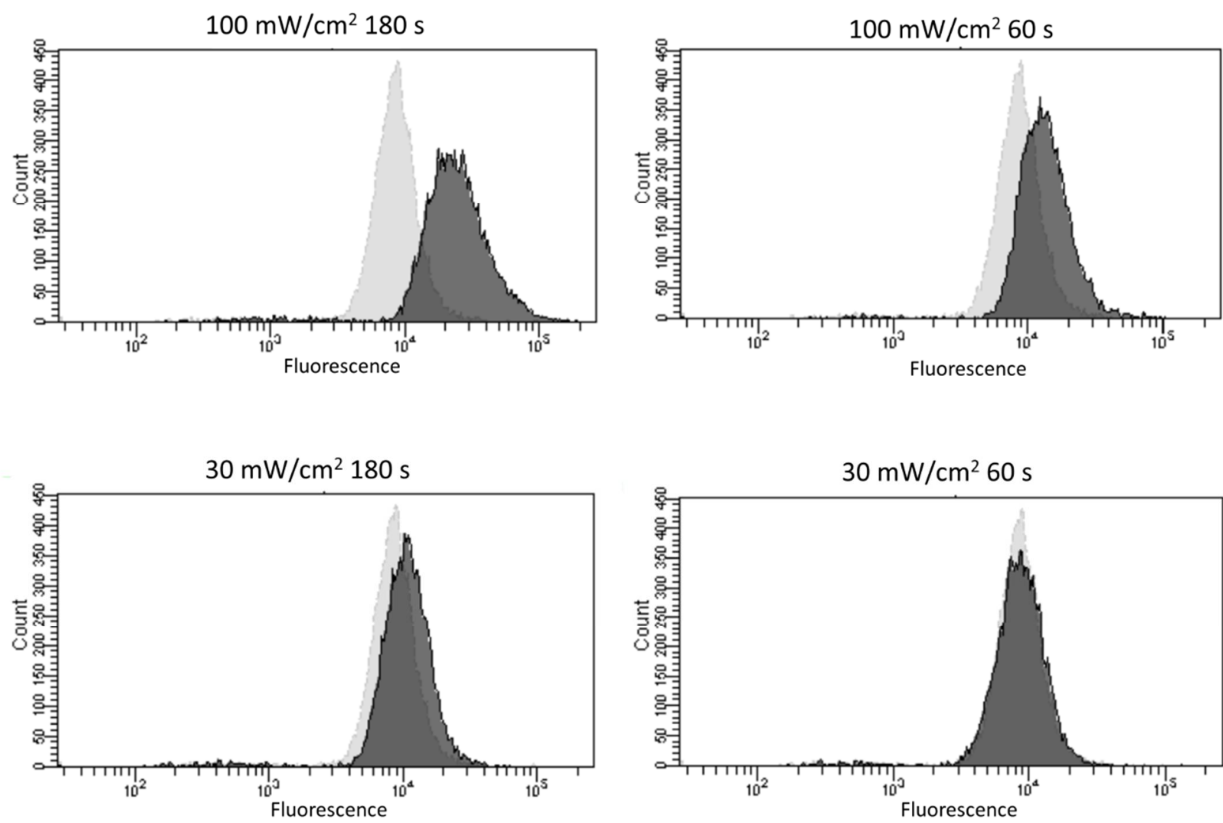


(a) OxiORANGE

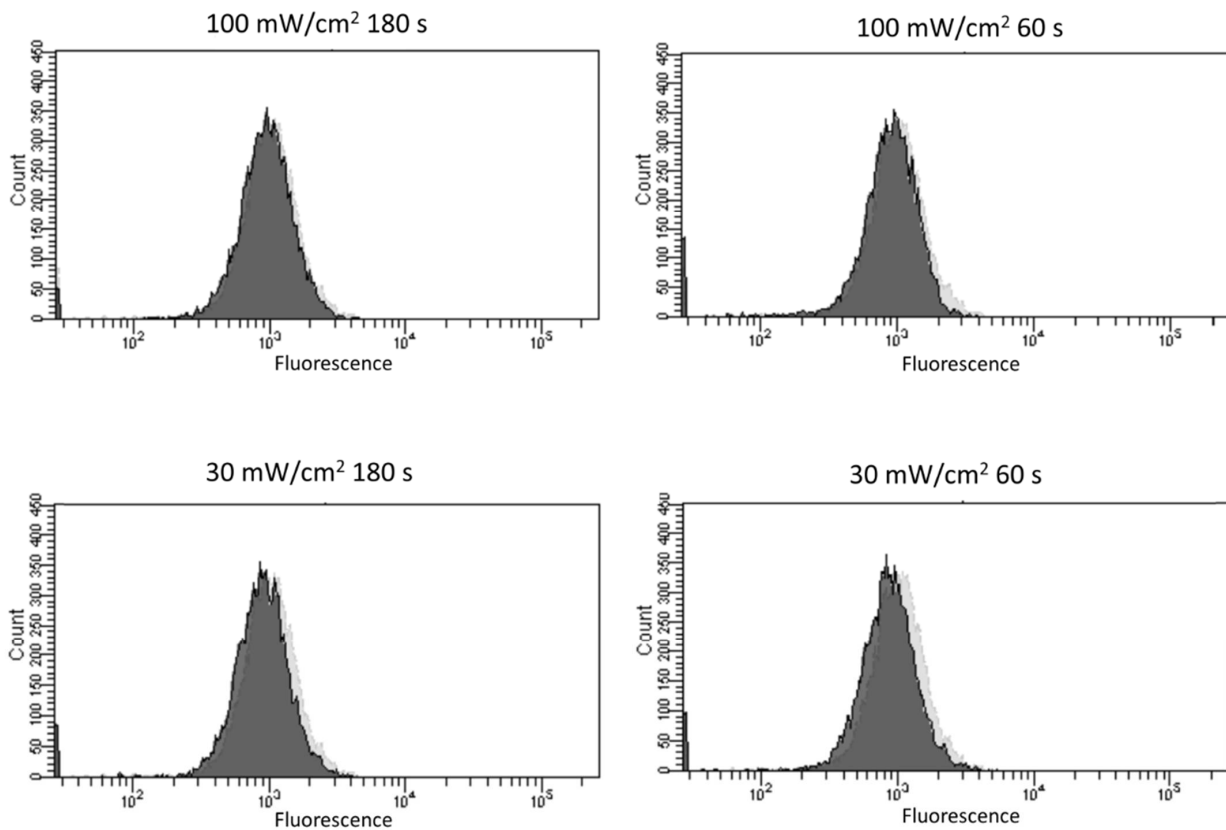


(b) HySOx

Figure 3. Cont.

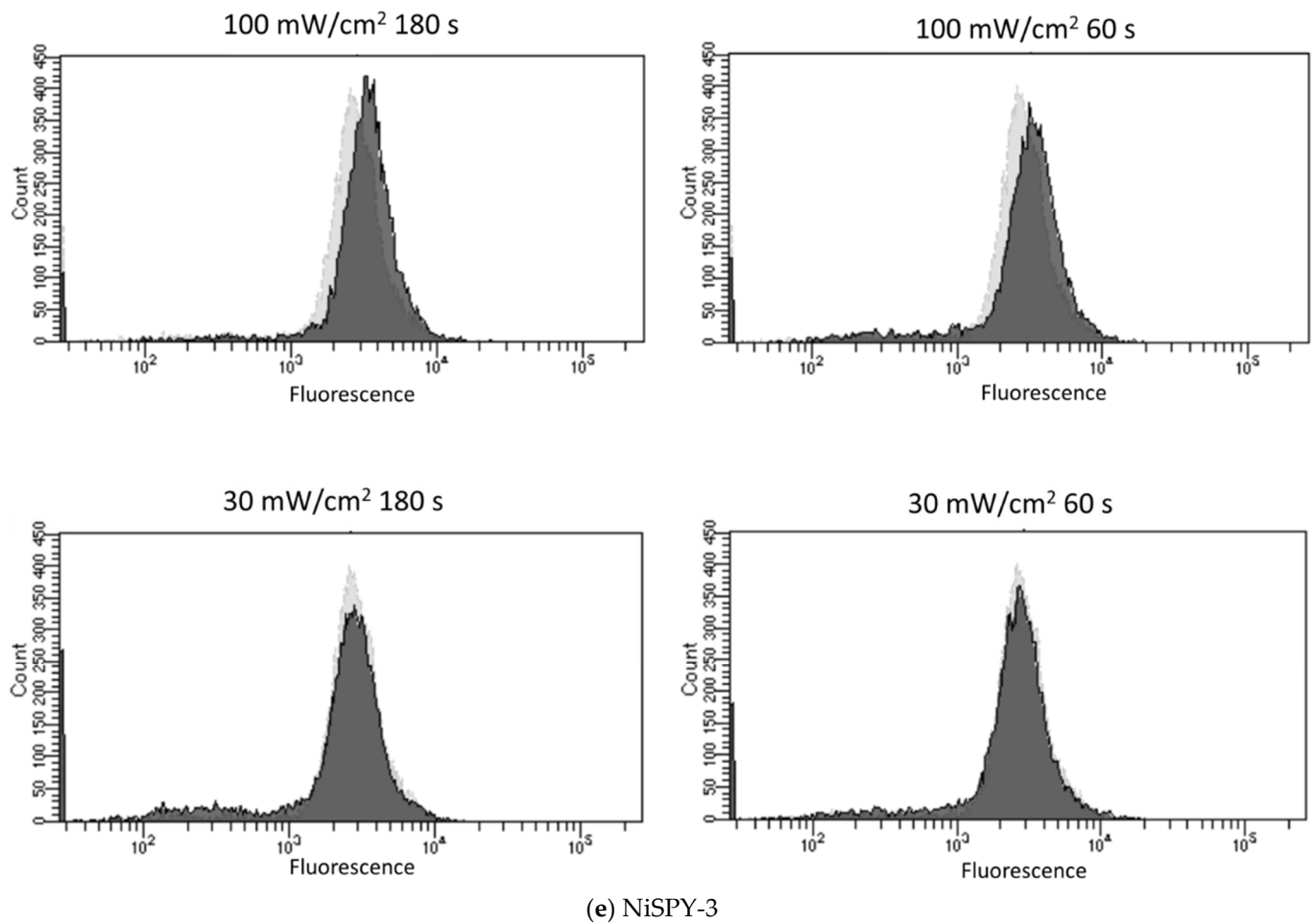


(c) Dihydroethidium



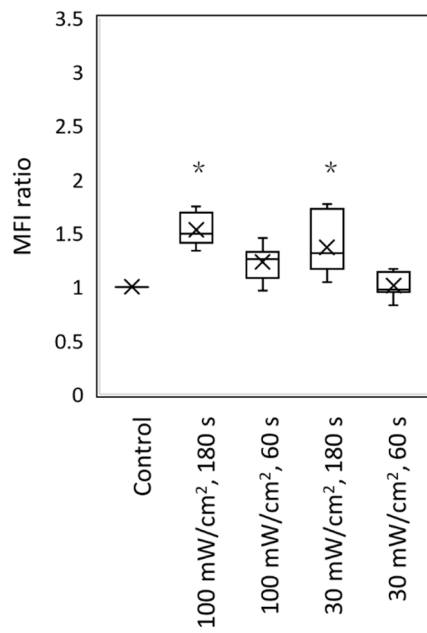
(d) Nitrixyte Red

Figure 3. Cont.

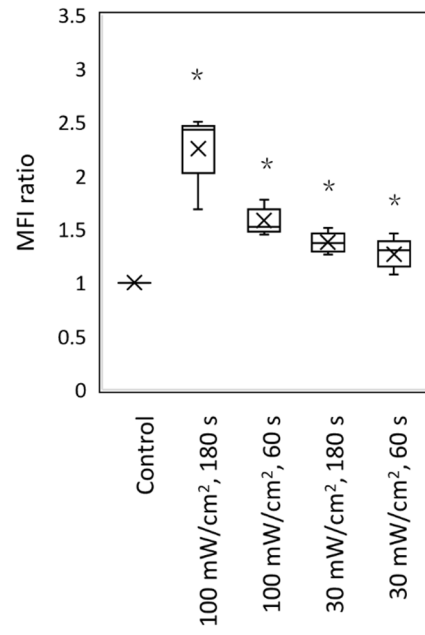


**Figure 3.** Representative histogram following blue laser irradiation obtained by flow cytometry. Five fluorescent probes were incorporated into the L929 mouse fibroblasts, and the cells were irradiated with a blue laser (405 nm). Each graph separately indicates the histogram for each fluorescent probe: (a) OxiORANGE (detects  $\bullet\text{OH}$  and  $\text{HClO}$ ), (b) HySOx (detects  $\text{HClO}$ ), (c) dihydroethidium (detects  $\text{O}_2^{\bullet-}$ ), (d) Nitrixyte Red (detects  $\text{NO}\bullet$ ), and (e) NiSPY-3 (detects  $\text{ONOO}^-$ ). The irradiation conditions were as follows: (1) control,  $100\text{ mW}/\text{cm}^2$ , 180 s, 18 J; (2)  $100\text{ mW}/\text{cm}^2$ , 60 s, 6 J; (3)  $30\text{ mW}/\text{cm}^2$ , 180 s, 5.4 J; (4)  $30\text{ mW}/\text{cm}^2$ , 60 s, 1.8 J. Light and dark gray histograms correspond to the control and irradiation groups, respectively.  $\bullet\text{OH}$ , hydroxyl radical;  $\text{HClO}$ , hypochlorous acid;  $\text{O}_2^{\bullet-}$ , superoxide anion;  $\text{NO}\bullet$ , nitric oxide;  $\text{ONOO}^-$ , peroxynitrite.

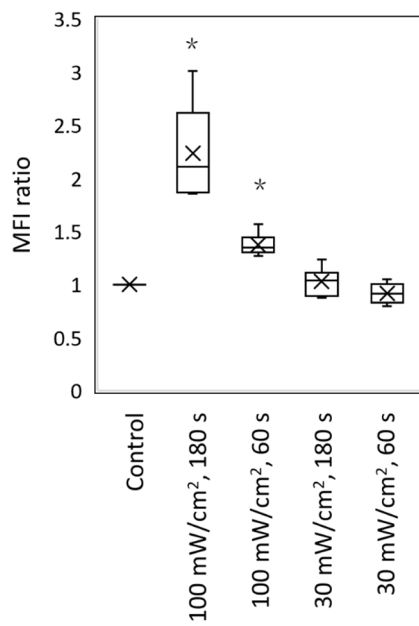
Figure 4 presents the MFI ratios for each fluorescent probe, which was calculated from the MFI obtained using flow cytometry. For OxiORANGE (detects  $\bullet\text{OH}$  and  $\text{HClO}$ ), the MFI ratio significantly increased under the following irradiation conditions: (1)  $100\text{ mW}/\text{cm}^2$ , 180 s, and (2)  $30\text{ mW}/\text{cm}^2$ , 180 s (Figure 4a). For HySOx (detects  $\text{HClO}$ ), the MFI ratio significantly increased under all irradiation conditions (Figure 4b), whereas for dihydroethidium (detects  $\text{O}_2^{\bullet-}$ ), the MFI ratio significantly increased under irradiation conditions of  $100\text{ mW}/\text{cm}^2$  for 180 s and  $100\text{ mW}/\text{cm}^2$  for 60 s (Figure 4c). For the Nitrixyte Red (detects of  $\text{NO}\bullet$ ), the MFI ratio slightly increased under irradiation conditions of  $30\text{ mW}/\text{cm}^2$  for 180 s and  $30\text{ mW}/\text{cm}^2$  for 60 s (Figure 4d). Finally, for the NiSPY-3 (detects of  $\text{ONOO}^-$ ), the MFI ratio slightly increased when irradiated at  $100\text{ mW}/\text{cm}^2$  for 180 s (Figure 4e).



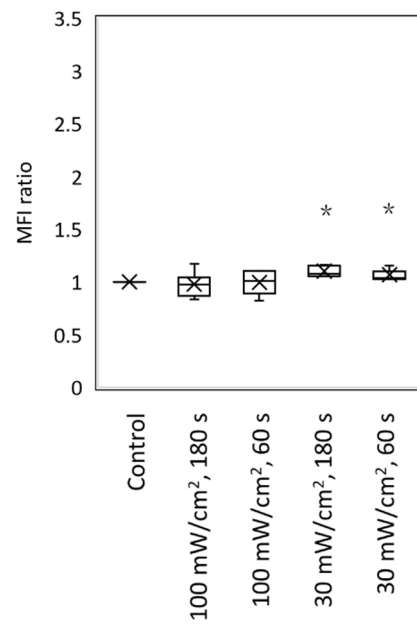
(a) OxiORANGE



(b) HySOx



(c) Dihydroethidium



(d) Nitroxyte Red

Figure 4. Cont.

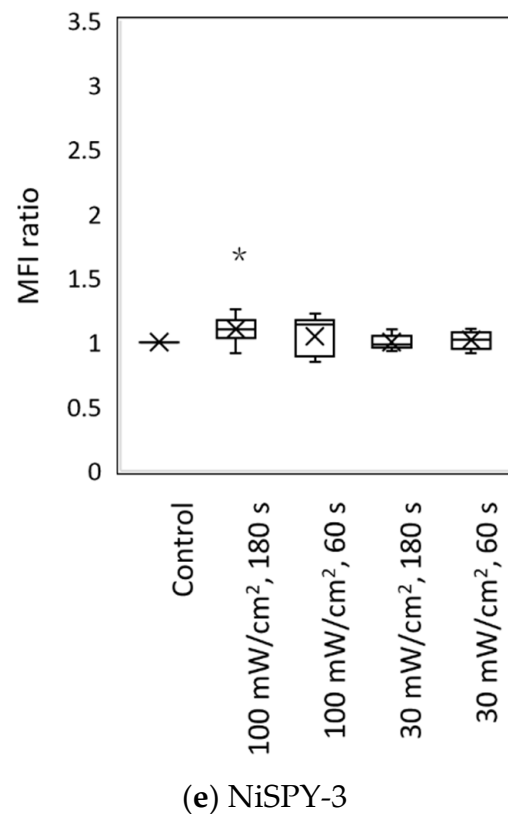


**Figure 4.** The MFI following blue laser irradiation. Five fluorescent probes were incorporated into the L929 mouse fibroblasts, and the cells were irradiated with a blue laser (405 nm). Each graph separately indicates the MFI ratio for each fluorescent probe: (a) OxiORANGE (detects  $\bullet\text{OH}$  and  $\text{HClO}$ ), (b) HySOx (detects  $\text{HClO}$ ), (c) dihydroethidium (detects  $\text{O}_2^- \bullet$ ), (d) Nitrixyte Red (detects  $\text{NO}\bullet$ ), and (e) NiSPY-3 (detects  $\text{ONOO}^-$ ). The irradiation conditions were as follows: (1) control, 100 mW/cm<sup>2</sup>, 180 s, 18 J; (2) 100 mW/cm<sup>2</sup>, 60 s, 6 J; 30 mW/cm<sup>2</sup>, 180 s, (3) 5.4 J; 30 mW/cm<sup>2</sup>, 60 s, 1.8 J. The MFIs of the positive control for each fluorescent probe (Table 1;  $n \geq 3$ ) were as follows: (a) OxiORANGE, 2.73; (b) HySOx, 44.46; (c) dihydroethidium, 3.21; (d) Nitrixyte Red, 2.95; (e) NiSPY-3, 1.99. The MFIs of the negative control (unstained cells) (Table 1;  $n \geq 3$ ) were as follows: (a) OxiORANGE, 0.66; (b) HySOx, 0.99; (c) dihydroethidium, 0.09; (d) Nitrixyte Red, 0.90; (e) NiSPY-3, 1.02. The MFI was measured using flow cytometry; the MFI ratio was calculated by dividing the MFI of irradiated cells with that of non-irradiated cells. \*  $p < 0.05$ .  $\bullet\text{OH}$ , hydroxyl radical;  $\text{HClO}$ , hypochlorous acid;  $\text{O}_2^- \bullet$ , superoxide anion;  $\text{NO}\bullet$ , nitric oxide;  $\text{ONOO}^-$ , peroxynitrite; MFI, mean fluorescence intensity.

### 3.3. Irradiation of a Blue Laser Reduces Cell Viability of L929 Cells

Cell viability assessment of L929 cells irradiated with a blue laser under various conditions was performed as follows: 100 mW/cm<sup>2</sup> for 180 s, 100 mW/cm<sup>2</sup> for 60 s, 30 mW/cm<sup>2</sup> for 180 s, and 30 mW/cm<sup>2</sup> for 60 s. At 4 h following MTT treatment, we observed significantly reduced cell viability under 100 mW/cm<sup>2</sup> for 180 s compared to that of the controls (Dunnett's multiple comparison tests; Figure 5).

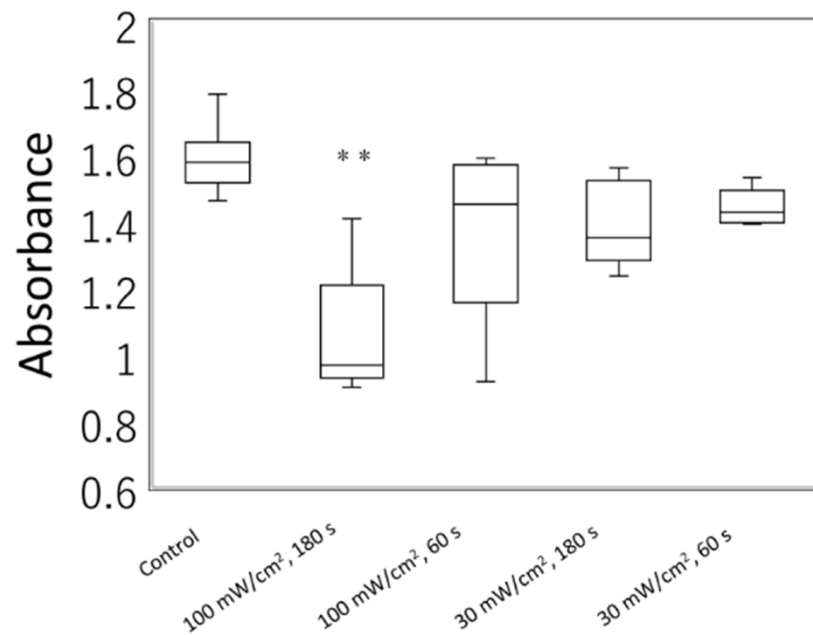


**Figure 5.** The cell viability assessment of irradiated cells. The 3-(4,5-dimethylthiazol-2-yl)-2,5-diphenyltetrazolium bromide (MTT) assay reagent was added at 24 h after the irradiation of L929 mouse fibroblasts with a blue laser of 405 nm, under various conditions (100 mW/cm<sup>2</sup>, 180 s, 18 J; 100 mW/cm<sup>2</sup>, 60 s, 6 J; 30 mW/cm<sup>2</sup>, 180 s, 5.4 J; 30 mW/cm<sup>2</sup>, 60 s, 1.8 J). Absorbance was measured at 4 h following MTT treatment. At least five independent experiments are presented. The results of the Kruskal–Wallis test followed by Dunnett’s multiple comparison tests showed a significant difference ( $p < 0.01$ ) among the five groups. \*\*  $p < 0.01$  against the control group.

#### 4. Discussion

As an indicator of oxidative stress, intracellular ATP concentration is associated with homeostasis of mitochondrial metabolism [24,25]. A decrease in the mitochondrial membrane potential may lead to a decrease in ATP production [26]. Thus, the decrease in the ATP level of the skin caused by blue laser irradiation may be attributed to mitochondrial damage caused by the ROS generation. In previous works, increases in ATP levels and other positive changes have been reported with low doses of blue light irradiation [27,28]. However, the irradiation conditions we employed in this experiment seemed to be more oxidatively stressful than those that could exert such a positive effect.

The mitochondrial respiratory chain constitutes the major intracellular ROS source in most tissues. The major ROS type that is generated in the mitochondria by univalent autoxidation of electron carriers is  $O_2^- \bullet$ . Superoxide dismutase (SOD) catalyzes the dismutation of  $O_2^- \bullet$ , thereby generating  $H_2O_2$ . Furthermore,  $H_2O_2$  reacts with redox-active metals, such as iron, to produce  $\bullet OH$  in a process called the Fenton/Haber–Weiss reaction [15,29].  $\bullet OH$  is a major cause of oxidative damage to DNA bases and is generated by various mechanisms.  $H_2O_2$  can also react with a chloride anion to form HClO, a reaction that requires myeloperoxidase. The latter is abundantly present in neutrophils, but it is also found in neuronal cells under certain conditions. HClO is a major end product of neutrophil respiratory burst. Endogenous HClO is a powerful natural oxidant that can react with proteins, DNA, RNA, fatty acids, and cholesterol, and plays vital physiological roles in living organisms [30]. To our knowledge, this is the first study to report blue light irradiation-induced HClO production in fibroblasts.

Several studies have reported  $NO \bullet$  generation by blue laser or red to near-infrared laser irradiation [31–33]. Irradiation of human skin with blue light (420–453 nm) at 58 mW/cm<sup>2</sup> for  $\geq 2$  min was shown to induce non-enzymatic nitric oxide generation from photo-labile nitric oxide derivatives in vitro and in vivo [34]. Lindgard et al. reported that the irradiation of human monocytes with a 634 nm LED at 35.7 W/cm<sup>2</sup> for 5 min

generated  $\text{NO}\bullet$  [31]. Moreover, near-infrared radiation has been shown to dissociate  $\text{NO}\bullet$  from cytochrome c oxidase, a key chromophore in PBM, and increase the intracellular  $\text{NO}\bullet$  levels in cardiomyocytes and HeLa cells [35]. Cytochrome c oxidase or Complex IV is a respiratory electron transport chain component. The application of light, particularly PBM, increases ATP production and electron transport [36]. Another RNS,  $\text{ONOO}^-$ , is produced by the diffusion-controlled reaction of  $\text{NO}\bullet$  and  $\text{O}_2^- \bullet$  [37].  $\text{ONOO}^-$  provides several beneficial effects and plays an auxiliary regulatory role in the immune system; however, its overproduction exerts harmful effects on the cell metabolism by inducing lipid peroxidation, DNA damage, and mitochondrial damage [16]. However, in our study, under irradiation conditions, we could not detect any RNS type, which could be attributed to the lower wavelength (405 nm) used compared with those of previous studies (>420 nm).

Blue light intracellular photoreceptors, including opsins, flavoproteins, and porphyrins, play important roles in the ROS and RNS generation. Opsin receptors (OPNs) are G protein-coupled receptors excited by blue or green light [28]. Human melanocytes and keratinocytes express four other opsins (i.e., OPN1-SW, OPN2, OPN3, and OPN5) [38]. OPN3 has also been detected in human fibroblasts [39]. Opening of light-gated ion channels, such as the transient receptor potential (TRP) family of calcium channels, is one of the best-defined signaling events that occurs after light-activation of opsins [40]. TRP activation results in nonselective permeabilization of the plasma membrane to calcium, sodium, and magnesium, possibly causing an increase in the intracellular calcium and consequently increasing the ROS and RNS, particularly  $\text{NO}\bullet$  [41]. Flavoproteins contain a riboflavin derivative (flavin adenine dinucleotide or flavin mononucleotide) as a prosthetic group and can be excited by blue light (400–500 nm) [42].  $\text{O}_2^- \bullet$  is generated by the photolytic intermediate of riboflavin, flavin mononucleotide, and flavin adenine dinucleotide [43]. Moreover, porphyrins have been observed in the human body [44]. Porphyrins have an absorption peak of approximately 418 nm, can absorb blue light, and generate  $^1\text{O}_2$  when excited to the triplet state [45]. Porphyrin precursors, such as 5-aminolevulinic acid, have been used in photodynamic therapy to kill cancer cells and vascular endothelial cells [46]. These reactions of porphyrins to blue light have been shown to account for the antibacterial properties of PBM [47]. Moreover, a wavelength of approximately 418 nm is commonly used for acne treatment. Despite the important role of these photoreceptors, we could not identify the specific photoreceptors involved in ROS generation under the experimental conditions. Therefore, further investigation is required.

Cells possess various enzymatic systems for detoxifying ROS. SOD catalyzes the conversion of  $\text{O}_2^- \bullet$  to  $\text{O}_2$  and  $\text{H}_2\text{O}_2$ . Although  $\text{O}_2^- \bullet$  is not very reactive, it reacts with the surrounding components to generate more reactive ROS, such as  $\text{ONOO}^-$  and  $\text{H}_2\text{O}_2$ .  $\text{O}_2^- \bullet$  oxidizes iron–sulfur clusters of proteins (such as the cytoplasmic enzymes, aconitase, and fumarase in the citric acid cycle), thereby degrading cluster iron and losing catalytic iron, resulting in enzyme inactivation [48]. Iron atoms released in this process directly reduce  $\text{H}_2\text{O}_2$  to produce more toxic  $\bullet\text{OH}$ . The majority of mitochondrial  $\text{H}_2\text{O}_2$  is generated by the disproportionation of  $\text{O}_2^- \bullet$  via MnSOD, which regulates the  $\text{O}_2^- \bullet$  levels and establishes the intracellular  $\text{H}_2\text{O}_2$  flux [49]. Therefore, SOD plays an integral role in controlling ROS and RNS concentrations in vivo [29]. We measured the total SOD activity after providing blue laser irradiation (Supplementary Figure S2). SOD activity is altered in response to various stimuli, but the time required for SOD activation varies [50,51].

In our study, the cells that received dihydroethidium presented significantly increased fluorescence with 405 nm laser irradiation at  $100 \text{ mW}/\text{cm}^2$ . Dihydroethidium reacts with  $\text{O}_2^- \bullet$  to produce 2-hydroxyethidium, a highly specific red fluorescence product. However, biological systems can react with other substances to form another red fluorescence product, ethidium. Moreover, dihydroethidium alone cannot completely identify superoxide [52]. Therefore, we should consider the involvement of various other ROS. Dihydroethidium does not react with singlet oxygen or  $\text{H}_2\text{O}_2$ ; however, this issue requires further investigation. Furthermore, this probe may underestimate  $\text{O}_2^- \bullet$  formation due to its short half-life and high rate of occurrence of the disproportionation reaction [53]. Therefore, we cannot

refute possible  $O_2^- \bullet$  generation below the detection limit under  $30 \text{ mW/cm}^2$  irradiation. ROS may act as signaling molecules at low concentrations and exhibit cytotoxic properties at high concentrations. A previous study involving irradiation of human fibroblasts using 410–480 nm blue light revealed that higher irradiation doses induced higher cytotoxicity, as evidenced by cell growth suppression [34]. Similarly, we observed a significant decrease in the cell viability assessment under  $100 \text{ mW/cm}^2$  irradiation for 180 s. Therefore, the 405 nm,  $100 \text{ mW/cm}^2$  laser irradiation for 180 s, which was provided in our experiment, may have caused certain damage.

Several studies have described blue light irradiation as a relatively reliable treatment method for acne [2]. However, no consensus exists on the light source wavelength, duration, and intensity of irradiation. The experimental conditions in our study were consistent with those of our previous study that detected ROS using blue light [22]. Additionally, the irradiation intensity was inferred from clinical trials that attempted to treat acne and psoriasis (approximately  $30\text{--}100 \text{ mW/cm}^2$ ). Furthermore, although treatments for acne vulgaris and psoriasis require longer irradiation periods, the effects of longer irradiation in *in vitro* studies could be drastic due to system sensitivity; therefore, we applied a shorter treatment duration. Moreover, considering that the skin has multiple cells and components that interact with each other, this finding cannot simply be applied *in vivo*, as the study was conducted only on fibroblasts. We inferred that excessively intense blue light irradiation could cause oxidative skin damage. However, detailed studies involving animal and human disease models are required to investigate the irradiation conditions that could exert maximal therapeutic effects with minimal oxidative stress.

We demonstrated that prolonged exposure to 405 nm laser irradiation significantly decreased the ATP levels in mouse skin and stimulated the production of HClO and  $O_2^- \bullet$ , whereas the generation of  $NO \bullet$  and  $ONOO^-$  was limited. Previous PBM studies have demonstrated the types of ROS and RNS that occur in various cells and tissues [9,11,12,54]. However, unlike our experiment, no attempts were made to detect multiple ROS and RNS simultaneously and systematically. Nevertheless, it is difficult to directly compare research results with those of other studies because there are various parameters, including the provided wavelength, irradiation density, irradiation time, and pulse width. Therefore, as noted in our research, investigating multiple ROS and RNS concurrently under certain conditions elucidates the individuality of irradiation conditions.

This study may serve as a basis for future research aimed at elucidating the formation mechanisms and subsequent reaction pathways of ROS and RNS. Our findings also highlight that oxidative stress from over-irradiation with blue light can cause adverse effects, such as aging. Furthermore, they may aid in the development of PBM-based therapeutic strategies. Further studies to investigate the most effective and harmless blue light irradiation conditions (wavelength, intensity, and time) using animal and human disease models are currently being performed in our laboratory.

## 5. Conclusions

Blue laser irradiation reduced the ATP levels in mouse skin and triggered the generation of  $O_2^-$ —and HClO. In addition, 405 nm blue laser irradiation at  $100 \text{ mW/cm}^2$  for 180 s decreased cell viability. These results suggest that caution is needed while using blue laser irradiation, as it could induce ROS production. Furthermore, our method of simultaneous measurement of ROS and RNS can be an appropriate experimental method to understand the characteristics of the complex irradiation conditions of PBM.

**Supplementary Materials:** The following is available online at <https://www.mdpi.com/article/10.3390/biology11020301/s1>, Supplementary Figure S1: Apoptosis in mouse fibroblasts (a) Irradiated tissue and (b) non-irradiated tissue, Supplementary Figure S2: Superoxide dismutase (SOD) activity in irradiated cells.

**Author Contributions:** Conceptualization, E.N. and T.K. (Toshihiro Kushibiki); Formal analysis, E.N.; Funding acquisition, T.K. (Toshihiro Kushibiki), R.A., M.I. and T.K. (Tomoharu Kiyosawa); Investigation, E.N. and Y.M.; Methodology, E.N. and T.K. (Toshihiro Kushibiki); Resources, M.I.; Writing—original draft, E.N.; Writing—review and editing, T.K. (Toshihiro Kushibiki). All authors have read and agreed to the published version of the manuscript.

**Funding:** This research received no external funding.

**Institutional Review Board Statement:** All animal experiments performed in this study were conducted in compliance with the ARRIVE guidelines, and the protocol was approved by the Ethics Committee for Animal Experiments of National Defense Medical College (approval number: 19010). All procedures were conducted according to relevant guidelines and regulations of National Defense Medical College.

**Data Availability Statement:** Data is contained within the article or Supplementary Material.

**Acknowledgments:** We would like to thank Professor Takahiro Nakamura, Department of Mathematics, National Defense Medical College, for providing advice regarding statistical analysis.

**Conflicts of Interest:** The authors declare no conflict of interest.

## References

1. Avci, P.; Gupta, A.; Sadasivam, M.; Vecchio, D.; Pam, Z.; Pam, N.; Hamblin, M.R. Low-level laser (light) therapy (LLLT) in skin: Stimulating, healing, restoring. *Semin. Cutan. Med. Surg.* **2013**, *32*, 41–52.
2. Scott, A.M.; Stehlik, P.; Clark, J.; Zhang, D.; Yang, Z.; Hoffmann, T.; Mar, C.D.; Glasziou, P. Blue-Light Therapy for Acne Vulgaris: A Systematic Review and Meta-Analysis. *Ann. Fam. Med.* **2019**, *17*, 545–553. [[CrossRef](#)]
3. Pfaff, S.; Liebmann, J.; Born, M.; Merk, H.F.; von Felbert, V. Prospective Randomized Long-Term Study on the Efficacy and Safety of UV-Free Blue Light for Treating Mild Psoriasis Vulgaris. *Dermatology* **2015**, *231*, 24–34. [[CrossRef](#)] [[PubMed](#)]
4. Yoshino, F.; Yoshida, A. Effects of blue-light irradiation during dental treatment. *Jpn. Dent. Sci. Rev.* **2018**, *54*, 160–168. [[CrossRef](#)] [[PubMed](#)]
5. Lee, S.Y.; You, C.E.; Park, M.Y. Blue and red light combination LED phototherapy for acne vulgaris in patients with skin phototype IV. *Lasers Surg. Med.* **2007**, *39*, 180–188. [[CrossRef](#)] [[PubMed](#)]
6. Elman, M.; Lebzelter, J. Light therapy in the treatment of acne vulgaris. *Dermatol. Surg.* **2004**, *30*, 139–146. [[CrossRef](#)]
7. Sadowska, M.; Narbutt, J.; Lesiak, A. Blue Light in Dermatology. *Life* **2021**, *11*, 670. [[CrossRef](#)]
8. Yoshida, A.; Yoshino, F.; Makita, T.; Maehata, Y.; Higashi, K.; Miyamoto, C.; Wada-Takahashi, S.; Takahashi, S.S.; Takahashi, O.; Lee, M.C. Reactive oxygen species production in mitochondria of human gingival fibroblast induced by blue light irradiation. *J. Photochem. Photobiol. B* **2013**, *129*, 1–5. [[CrossRef](#)]
9. Nakashima, Y.; Ohta, S.; Wolf, A.M. Blue light-induced oxidative stress in live skin. *Free Radic. Biol. Med.* **2017**, *108*, 300–310. [[CrossRef](#)]
10. Hamblin, M.R. Mechanisms and Mitochondrial Redox Signaling in Photobiomodulation. *Photochem. Photobiol.* **2018**, *94*, 199–212. [[CrossRef](#)]
11. Nakanishi-Ueda, T.; Majima, H.J.; Watanabe, K.; Ueda, T.; Indo, H.P.; Suenaga, S.; Hisamitsu, T.; Ozawa, T.; Yasuhara, H.; Koide, R. Blue LED light exposure develops intracellular reactive oxygen species, lipid peroxidation, and subsequent cellular injuries in cultured bovine retinal pigment epithelial cells. *Free Radic. Res.* **2013**, *47*, 774–780. [[CrossRef](#)]
12. Arthaut, L.D.; Jourdan, N.; Mteyrek, A.; Procopio, M.; El-Esawi, M.; d’Harlingue, A.; Bouchet, P.E.; Witczak, J.; Ritz, T.; Klarsfeld, A.; et al. Blue-light induced accumulation of reactive oxygen species is a consequence of the Drosophila cryptochrome photocycle. *PLoS ONE* **2017**, *12*, e0171836. [[CrossRef](#)] [[PubMed](#)]
13. Kudryavtseva, A.V.; Krasnov, G.S.; Dmitriev, A.A.; Alekseev, B.Y.; Kardymon, O.L.; Sadritdinova, A.F.; Fedorova, M.S.; Pokrovsky, A.V.; Melnikova, N.V.; Kaprin, A.D.; et al. Mitochondrial dysfunction and oxidative stress in aging and cancer. *Oncotarget* **2016**, *7*, 44879–44905. [[CrossRef](#)] [[PubMed](#)]
14. Karu, T.I. Mitochondrial signaling in mammalian cells activated by red and near-IR radiation. *Photochem. Photobiol.* **2008**, *84*, 1091–1099. [[CrossRef](#)] [[PubMed](#)]
15. Di Meo, S.; Reed, T.T.; Venditti, P.; Victor, V.M. Role of ROS and RNS Sources in Physiological and Pathological Conditions. *Oxid. Med. Cell. Longev.* **2016**, *2016*, 1245049. [[CrossRef](#)] [[PubMed](#)]
16. Adams, L.; Franco, M.C.; Estevez, A.G. Reactive nitrogen species in cellular signaling. *Exp. Biol. Med. (Maywood)* **2015**, *240*, 711–717. [[CrossRef](#)] [[PubMed](#)]
17. Liu, H.; Colavitti, R.; Rovira, I.I.; Finkel, T. Redox-dependent transcriptional regulation. *Circ. Res.* **2005**, *97*, 967–974. [[CrossRef](#)] [[PubMed](#)]
18. Gao, X.; Xing, D. Molecular mechanisms of cell proliferation induced by low power laser irradiation. *J. Biomed. Sci.* **2009**, *16*, 4. [[CrossRef](#)]

19. Wu, J.Y.; Chen, C.H.; Wang, C.Z.; Ho, M.L.; Yeh, M.L.; Wang, Y.H. Low-power laser irradiation suppresses inflammatory response of human adipose-derived stem cells by modulating intracellular cyclic AMP level and NF-kappaB activity. *PLoS ONE* **2013**, *8*, e54067. [[CrossRef](#)]
20. Jagdeo, J.; Austin, E.; Mamalis, A.; Wong, C.; Ho, D.; Siegel, D.M. Light-emitting diodes in dermatology: A systematic review of randomized controlled trials. *Lasers Surg. Med.* **2018**, *50*, 613–628. [[CrossRef](#)]
21. Diogo, M.L.G.; Campos, T.M.; Fonseca, E.S.R.; Pavani, C.; Horliana, A.; Fernandes, K.P.S.; Bussadori, S.K.; Fantin, F.; Leite, D.P.V.; Yamamoto, A.T.A.; et al. Effect of Blue Light on Acne Vulgaris: A Systematic Review. *Sensors* **2021**, *21*, 6943. [[CrossRef](#)]
22. Kushibiki, T.; Hirasawa, T.; Okawa, S.; Ishihara, M. Blue laser irradiation generates intracellular reactive oxygen species in various types of cells. *Photomed. Laser Surg.* **2013**, *31*, 95–104. [[CrossRef](#)] [[PubMed](#)]
23. Kushibiki, T.; Hirasawa, T.; Okawa, S.; Ishihara, M. Low Reactive Level Laser Therapy for Mesenchymal Stromal Cells Therapies. *Stem Cells Int.* **2015**, *2015*, 974864. [[CrossRef](#)]
24. Park, C.; Cha, H.J.; Hong, S.H.; Kim, G.Y.; Kim, S.; Kim, H.S.; Kim, B.W.; Jeon, Y.J.; Choi, Y.H. Protective Effect of Phloroglucinol on Oxidative Stress-Induced DNA Damage and Apoptosis through Activation of the Nrf2/HO-1 Signaling Pathway in HaCaT Human Keratinocytes. *Mar. Drugs* **2019**, *17*, 225. [[CrossRef](#)] [[PubMed](#)]
25. Jiang, D.; Fu, C.; Xiao, J.; Zhang, Z.; Zou, J.; Ye, Z.; Zhang, X. SGK1 Attenuates Oxidative Stress-Induced Renal Tubular Epithelial Cell Injury by Regulating Mitochondrial Function. *Oxid. Med. Longev.* **2019**, *2019*, 2013594. [[CrossRef](#)]
26. Cui, L.; Li, Z.; Chang, X.; Cong, G.; Hao, L. Quercetin attenuates vascular calcification by inhibiting oxidative stress and mitochondrial fission. *Vasc. Pharmacol.* **2017**, *88*, 21–29. [[CrossRef](#)] [[PubMed](#)]
27. Al Musawi, M.S.; Al-Gailani, B.T. ATP level in red blood cells improves by altering the low-level DPSS laser irradiation condition. *Appl. Nanosc.* **2021**. [[CrossRef](#)]
28. Buscone, S.; Mardaryev, A.N.; Raafs, B.; Bikker, J.W.; Sticht, C.; Gretz, N.; Farjo, N.; Uzunbajakava, N.E.; Botchkareva, N.V. A new path in defining light parameters for hair growth: Discovery and modulation of photoreceptors in human hair follicle. *Lasers Surg. Med.* **2017**, *49*, 705–718. [[CrossRef](#)]
29. Wang, Y.; Branicky, R.; Noe, A.; Hekimi, S. Superoxide dismutases: Dual roles in controlling ROS damage and regulating ROS signaling. *J. Cell Biol.* **2018**, *217*, 1915–1928. [[CrossRef](#)]
30. Hawkins, C.L.; Pattison, D.I.; Davies, M.J. Hypochlorite-induced oxidation of amino acids, peptides and proteins. *Amino Acids* **2003**, *25*, 259–274. [[CrossRef](#)]
31. Lindgard, A.; Hulten, L.M.; Svensson, L.; Soussi, B. Irradiation at 634 nm releases nitric oxide from human monocytes. *Lasers Med. Sci.* **2007**, *22*, 30–36. [[CrossRef](#)] [[PubMed](#)]
32. Rizzi, M.; Migliario, M.; Tonello, S.; Rocchetti, V.; Reno, F. Photobiomodulation induces in vitro re-epithelialization via nitric oxide production. *Lasers Med. Sci.* **2018**, *33*, 1003–1008. [[CrossRef](#)] [[PubMed](#)]
33. Zhang, R.; Mio, Y.; Pratt, P.F.; Lohr, N.; Warltier, D.C.; Whelan, H.T.; Zhu, D.; Jacobs, E.R.; Medhora, M.; Bienengraeber, M. Near infrared light protects cardiomyocytes from hypoxia and reoxygenation injury by a nitric oxide dependent mechanism. *J. Mol. Cell. Cardiol.* **2009**, *46*, 4–14. [[CrossRef](#)] [[PubMed](#)]
34. Oplander, C.; Hidding, S.; Werners, F.B.; Born, M.; Pallua, N.; Suschek, C.V. Effects of blue light irradiation on human dermal fibroblasts. *J. Photochem. Photobiol. B* **2011**, *103*, 118–125. [[CrossRef](#)] [[PubMed](#)]
35. Karu, T.I.; Pyatibrat, L.V.; Afanasyeva, N.I. Cellular effects of low power laser therapy can be mediated by nitric oxide. *Lasers Surg. Med.* **2005**, *36*, 307–314. [[CrossRef](#)] [[PubMed](#)]
36. Chung, H.; Dai, T.; Sharma, S.K.; Huang, Y.Y.; Carroll, J.D.; Hamblin, M.R. The nuts and bolts of low-level laser (light) therapy. *Ann. Biomed. Eng.* **2012**, *40*, 516–533. [[CrossRef](#)]
37. Nausier, T.; Koppenol, W. The Rate Constant of the Reaction of Superoxide with Nitrogen Monoxide: Approaching the Diffusion Limit. *J. Phys. Chem. A* **2002**, *106*, 4084–4086. [[CrossRef](#)]
38. Terakita, A. The opsins. *Genome Biol.* **2005**, *6*, 213. [[CrossRef](#)]
39. Castellano-Pellicena, I.; Uzunbajakava, N.E.; Mignon, C.; Raafs, B.; Botchkarev, V.A.; Thornton, M.J. Does blue light restore human epidermal barrier function via activation of Opsin during cutaneous wound healing? *Lasers Surg. Med.* **2019**, *51*, 370–382. [[CrossRef](#)]
40. Poletini, M.O.; Moraes, M.N.; Ramos, B.C.; Jeronimo, R.; Castrucci, A.M. TRP channels: A missing bond in the entrainment mechanism of peripheral clocks throughout evolution. *Temperature (Austin)* **2015**, *2*, 522–534. [[CrossRef](#)]
41. Wang, Y.; Huang, Y.Y.; Wang, Y.; Lyu, P.; Hamblin, M.R. Red (660 nm) or near-infrared (810 nm) photobiomodulation stimulates, while blue (415 nm), green (540 nm) light inhibits proliferation in human adipose-derived stem cells. *Sci. Rep.* **2017**, *7*, 7781. [[CrossRef](#)]
42. Swartz, T.E.; Corchnoy, S.B.; Christie, J.M.; Lewis, J.W.; Szundi, I.; Briggs, W.R.; Bogomolni, R.A. The photocycle of a flavin-binding domain of the blue light photoreceptor phototropin. *J. Biol. Chem.* **2001**, *276*, 36493–36500. [[CrossRef](#)] [[PubMed](#)]
43. Yang, M.Y.; Chang, C.J.; Chen, L.Y. Blue light induced reactive oxygen species from flavin mononucleotide and flavin adenine dinucleotide on lethality of HeLa cells. *J. Photochem. Photobiol. B* **2017**, *173*, 325–332. [[CrossRef](#)] [[PubMed](#)]
44. Shu, M.; Kuo, S.; Wang, Y.; Jiang, Y.; Liu, Y.T.; Gallo, R.L.; Huang, C.M. Porphyrin metabolisms in human skin commensal *Propionibacterium acnes* bacteria: Potential application to monitor human radiation risk. *Curr. Med. Chem.* **2013**, *20*, 562–568. [[CrossRef](#)] [[PubMed](#)]

45. Tsolekile, N.; Nelana, S.; Oluwafemi, O.S. Porphyrin as Diagnostic and Therapeutic Agent. *Molecules* **2019**, *24*, 2669. [[CrossRef](#)] [[PubMed](#)]
46. Krammer, B.; Plaetzer, K. ALA and its clinical impact, from bench to bedside. *Photochem. Photobiol. Sci.* **2008**, *7*, 283–289. [[CrossRef](#)] [[PubMed](#)]
47. Amin, R.M.; Bhayana, B.; Hamblin, M.R.; Dai, T. Antimicrobial blue light inactivation of *Pseudomonas aeruginosa* by photo-excitation of endogenous porphyrins: In vitro and in vivo studies. *Lasers Surg. Med.* **2016**, *48*, 562–568. [[CrossRef](#)] [[PubMed](#)]
48. Imlay, J.A. Pathways of oxidative damage. *Annu. Rev. Microbiol.* **2003**, *57*, 395–418. [[CrossRef](#)]
49. Buettner, G.R. Superoxide dismutase in redox biology: The roles of superoxide and hydrogen peroxide. *Anticancer Agents Med. Chem.* **2011**, *11*, 341–346. [[CrossRef](#)]
50. Wiecek, M.; Szymura, J.; Maciejczyk, M.; Kantorowicz, M.; Szygula, Z. Anaerobic Exercise-Induced Activation of Antioxidant Enzymes in the Blood of Women and Men. *Front. Physiol.* **2018**, *9*, 1006. [[CrossRef](#)]
51. Roehlecke, C.; Schumann, U.; Ader, M.; Brunssen, C.; Bramke, S.; Morawietz, H.; Funk, R.H. Stress reaction in outer segments of photoreceptors after blue light irradiation. *PLoS ONE* **2013**, *8*, e71570. [[CrossRef](#)] [[PubMed](#)]
52. Zielonka, J.; Kalyanaraman, B. Hydroethidine- and MitoSOX-derived red fluorescence is not a reliable indicator of intracellular superoxide formation: Another inconvenient truth. *Free Radic. Biol. Med.* **2010**, *48*, 983–1001. [[CrossRef](#)] [[PubMed](#)]
53. Chen, J.; Rogers, S.C.; Kavdia, M. Analysis of kinetics of dihydroethidium fluorescence with superoxide using xanthine oxidase and hypoxanthine assay. *Ann. Biomed. Eng.* **2013**, *41*, 327–337. [[CrossRef](#)] [[PubMed](#)]
54. Yoshida, A.; Shiotsu-Ogura, Y.; Wada-Takahashi, S.; Takahashi, S.S.; Toyama, T.; Yoshino, F. Blue light irradiation-induced oxidative stress in vivo via ROS generation in rat gingival tissue. *J. Photochem. Photobiol. B* **2015**, *151*, 48–53. [[CrossRef](#)]